

# Elasticity of the PCF-graphene-based single-layer and nanotubes performed by state-of-the-art of reactive classical molecular dynamics simulation method

Reza Kalami <sup>a,\*</sup>, Seyed Ahmad Ketabi <sup>a,\*</sup>, José M. De Sousa <sup>b,\*</sup>

<sup>a</sup>*School of Physics, Damghan University, Damghan, Iran*

<sup>b</sup>*Instituto Federal de Educação, Ciência e Tecnologia do Piauí – IFPI, Primavera, São Raimundo Nonato, 64770-000, Piauí, Brazil*

---

## Abstract

A novel two-dimensional carbon allotrope called PCF-graphene has been theoretically proposed. The development of its nanostructured morphology has arrangement a non-aromatic molecule cyclooctatetraene as a precursor (poly-cyclooctatetraene framework). This new carbon allotrope is purely  $sp^2$ -hybridized carbon atoms. In the first-principles calculations, PCF-graphene are thermally, mechanically, and dynamically stable. With a finite thickness of 2.45Å, PCF-graphene is a semiconductor with a direct band gap of 0.77 eV. Exhibits anisotropies in elastic properties, carrier mobility, and optical absorption. Despite having been proposed recently, the study of the mechanical properties of single-layer and nanotubes of PCF-graphene has not been developed yet. Thus, our motivation in this work is to study the mechanical properties of PCF-graphene single-layer and nanotubes. Using state-of-the-art of the fully atomistic classical molecular dynamics simulations method with the use of the interatomic potential ReaxFF implemented in the LAMMPS code, we intend to study the mechanical properties of PCF-graphene 1D and 2D. Our results showed that, the Young's Modulus for PCF-graphene single-layer for uniaxial strain in the  $x$ -direction ranges from 5651.7 – 4328.6 GPa.Å and in the  $y$ -direction 2408.5 – 1934.4 GPa.Å. The Young's modulus of the PCF-G-NTs ((0,  $n$ ) and ( $n$ , 0)) are range 1850.5 – 2603.3 GPa.Å and, 386.25 – 1280.7 GPa.Å, respectively. The Poisson's coefficients value are 0.20 and 0.48 for PCF-G-NTs (6, 0) and (0, 7), respectively. We believe that the new results presented to the scientific community in nanoscience can contribute to a theoretical library for future applications of the PCF-graphene nanostructure in the sustained development of new electromechanical devices and new carbon-based materials.

**Keywords:** Classical molecular dynamics simulations method, reactive interatomic force field - ReaxFF, PCF-graphene, elastic properties, nanofracture pattern

---

\*Corresponding authors: rezakk01@gmail.com (R. Kalami), saketabi@du.ac.ir (S. A. Ketabi), josemoreiradesousa@ifpi.edu.br (J. M. De Sousa).

## 1. Introduction

The carbon allotropy originates several materials, but the only ones occurring in nature are graphite and diamond. Carbon is one of the elements that perform the allotropy phenomenon, that is, it bonds in different ways, forming several simple nanostructures with different physical and chemical shapes and properties. Thus, carbon is able to form many allotropic forms due to its valence [1, 2].

Due to carbon allotropy, the possibilities of new nanostructures and their applications in nanoscience and nanotechnology are possible to be obtained theoretically and experimentally. In recent decades, many more allotropes and forms of carbon have been discovered and researched theoretically and experimentally, including graphene. Graphene, as single sheet of graphite, was synthesized and isolated by mechanical exfoliation [3]. Graphene is a zero-gap semiconductor, which limits its applications in some electronic devices including digital transistors [4]. One of the ways to overcome this problem is to open the electronic gap of graphene, in a controlled way, preserving the electronic properties of graphene [3, 4]. Several attempts were made to open the electronic gap of graphene, such as the process of chemical functionalization [5, 6, 7, 8], strain based gap engineering, applying the electric field and other methods and technologies that can affect the structural symmetries. However, the recently proposals of new allotropic carbon nanostructures which inherently have a certain energy gap with the semiconducting properties and qualities equal to or superior to graphene has opened new perspectives for the design of graphene-based optoelectronic devices. One of such interesting families of carbon allotropes is called Graphyne, represented by 2D-like forming three hybridization states ( $sp^3$ ,  $sp^2$ , and  $sp^1$ ) hybridized carbon [9, 10]. Unlike graphene, the graphyne nanostructures are semiconductors with direct transitions range from 0.46 to 1.22 eV. The elastic modulus of graphyne are range  $170 - 240 Nm^{-1}$ . The bending stiffness of graphyne is estimated to be approximately 1.68 eV [11]. Another recently studied allotrope of carbon is penta-graphene which is composed entirely of carbon pentagons and  $sp^2$  and  $sp^3$  hybridized carbon atoms. Sheet of penta-graphene has an indirect band gap of 4.1 – 4.3 eV. Due to its morphology configuration (half-thickness being  $h = 0.6\text{\AA}$ ), penta-graphene has an elastic properties of the 150.5 GPa.nm, UTS of the 38 GPa.nm and  $\sigma_c = 20\%$  [12]. Theoretical studies developed by classical molecular dynamics method with the interatomic reactive potential ReaxFF, analyzed the effects of temperature on the elastic properties of penta-graphene single-layer. The results obtained showed that penta-graphene thermalized up to 2000 K, so that the strain rate was reduced to 67%, reduction in UTS 35.88 – 11.83 GPa.nm and Young's Modulus of the 227.15 – 154.76 GPa.nm [13]. The elasticity of penta-graphene-based nanotube has been studied theoretically by density functional theory (DFT) and reactive (ReaxFF) classical molecular dynamics method (CMD). The results indicate that the elastic modulus values are in the range of 680 – 800 GPa, UTS of the 85 – 110 GPa and  $\sigma_C = 18 - 21\%$  [14].

Another interesting allotrope of carbon is called Poly-Cyclooctatetraene Framework (PCF)-graphene [15]. This new carbon allotrope has a direct band gap of 0.77 eV. It is similar to the  $sp^2$ -hybridized carbon atoms in graphene (see Fig. 1). Calculations performed by first principles ab initio method showed that PCF-graphene is nanostructurally stable

(thermally, mechanically, and dynamically), and exhibits anisotropic optical adsorption and elasticity [15]. Despite having been proposed recently, the study of the elasticity properties of PCF-graphene-based single-layer and nanotubes has not been developed yet. Thus, the purpose of this work is to study the elasticity properties of PCF-graphene single-layer (at temperatures of the 10 up to 1200 K) and nanotubes (PCF-G-NTs) at room temperature, performed by state-of-the-art of reactive (ReaxFF) classical molecular dynamics simulation method. The results obtained showed that the Young’s Modulus for PCF-graphene single-layer for uniaxial strain in the  $x$ -direction ranges from  $5651.7 - 4328.6$  GPaÅ and in the  $y$ -direction  $2408.5 - 1934.4$  GPaÅ, considering the thickness of  $3.35$  Å. The Young’s modulus of the PCF-G-NTs ( $(0, n)$  and  $(n, 0)$ ) are range  $1850.5 - 2603.3$  GPaÅ and,  $386.25 - 1280.7$  GPaÅ, respectively.

In section 1, we briefly introduced the preliminary concepts and the motivations for the development of this theoretical work. In sections 2 and 3 we present the computational methodology used to model the nanostructures of PCF-graphene-based single-layer and nanotubes. The results and discussion are presented in Section 4 followed by conclusions and remarks in Section 5.

## 2. Computational Methodology

The reactive molecular dynamics simulations method were carried out to study the tensile stress/strain behavior of PCF-graphene single-layer and nanotube (PCF-G-NTs). These reactive molecular dynamics simulations were performed using the LAMMPS (Large-scale Atomic/Molecular Massively Parallel Simulator) [16] code with the interatomic reactive Force Field (ReaxFF) [17]. ReaxFF is a interatomic reactive force field developed by van Duin, Goddard III and co-workers for using in molecular dynamics method calculations.

The system energy is divided into partial energy contributions, such as, bond distance ( $E_{bond}$ ), the over-coordination ( $E_{over}$ ), the under-coordination ( $E_{under}$ ), the valence ( $E_{val}$ ), the penalty for handling atoms with two double bonds ( $E_{pen}$ ), the torsion ( $E_{tor}$ ), the conjugated bond energies ( $E_{conj}$ ), the van der Waals ( $E_{vdW}$ ), and coulomb interactions ( $E_{co}$ ). The ReaxFF can handle bond formation and dissociation, making and breaking bonds, as a function of bond order values. ReaxFF was parametrized with DFT calculations, being the average deviation between the heats of formation predicted by the theory and by the experiment equal to 2.8 and 2.9  $kcal\ mol^{-1}$ , for non-conjugated and conjugated systems. ReaxFF has been successfully used in the study of elastic properties of nanostructured systems [18, 19, 20], among other nanostructures.

The nanostructural model of the PCF-graphene single-layer (shown in Figure 1) consists of 14400 carbon atoms and has dimensions of  $146.22 \times 163.23$  Å<sup>2</sup>. Nanostructural details of the (PCF-G-NTs) are presented in Table 1. Before coupling the thermostat chain on the PCF-graphene single-layer and nanotubes (PCF-G-NTs) for thermodynamic equilibrium before starting the mechanical stretching process, all nanostructures studied in this work are initially subjected to carbon atoms restrained energy minimization with respect to both the torsion angles and the atomic Cartesian co-ordinates. Before starting the stretch processes, in order to eliminate any residual stress present on the all nanostructures, we perform constant

*NPT* integration thermalization carried at null pressure using a Nose/Hoover pressure barostat during 10000 fs [21]. Then, the tensile mechanical were performed by stretching the PCF-graphene single-layer and nanotubes (PCF-G-NTs) until nanofracture within NVT ensemble (Nose/Hoover temperature thermostat) at room temperature during 10000 fs. In all reactive molecular dynamics simulations we use a timestep of 0.05 fs. We used a constant engineering tensile strain rate  $\delta = 10^{-6} f s^{-1}$ .

The elastic properties of the PCF-graphene single-layer and nanotubes (PCF-G-NTs) were analyzed by the stress-strain relationship, where the engineering strain,  $\varepsilon$ , under tension is defined as

$$\varepsilon = \frac{\zeta - \zeta_0}{\zeta_0} = \frac{\Delta\zeta}{\zeta_0}, \quad (1)$$

where  $\zeta_0$  and  $\zeta$  are the length of the structure before and after the dynamics of deformation, respectively. The *per-atom* stress tensor of each carbon atom are calculated by [22]:

$$\sigma_{\alpha\beta} = \Gamma^{-1} \sum_i^N (m_i v_{\alpha i} v_{i\beta} + r_{i\alpha} f_{i\beta}), \quad (2)$$

where  $\Gamma$  is the atom volume,  $N$  the number of atoms,  $m_i$  the mass of carbon atoms,  $v$  the velocity,  $r$  the coordinates of the carbon atoms and  $f_{i\beta}$  is the  $\beta$  component of the force acting on the  $i$ -th atom. In order to perform a more detailed analysis of the distribution of stress along the structure during the fracture process, we also calculated the quantity known as *von Mises stress*,  $\sigma_{vM}$ , which is mathematically given by [22]:

$$\sigma_{vM} = \sqrt{\left[ \frac{(\sigma_{xx} - \sigma_{yy})^2 + (\sigma_{yy} - \sigma_{zz})^2 + (\sigma_{zz} - \sigma_{xx})^2 + 6(\tau_{xy}^2 + \tau_{yz}^2 + \tau_{zx}^2)}{2} \right]}, \quad (3)$$

where  $\sigma_{xy}$ ,  $\sigma_{yz}$  and  $\sigma_{zx}$  are shear stress components. The  $\tau_{xy}$ ,  $\tau_{yz}$  and  $\tau_{zx}$  are shear stress components. It allows a dynamical visualization (qualitatively) of where the stress is accumulated and dissipated during the stretching and nanofracture process along the whole nanostructure of PCF-graphene-based single-layer and nanotubes (PCF-G-NTs).

### 2.1. Calculation of Poisson's ratio of the PCF-graphene-based nanotubes (PCF-G-NTs)

The cylindrical nanostructural shape of PCF-graphene-based carbon nanotubes (PCF-G-NTs) theoretically investigated in this research work, the PCF-G-NTs are subjected at uniaxial strain load in  $z$ -direction, ( $\varepsilon$ ), without the radial constraint. Thus, the evaluated Poisson's ratio is mathematically given by the following expression [23]:

$$\nu = -\lim_{\varepsilon \rightarrow 0} \left( \frac{\varepsilon'}{\varepsilon} \right), \quad (4)$$

where,  $\nu$  Poisson's ratio,  $\varepsilon'$  radial strain and  $\varepsilon$  uniaxial strain applied in PCF-G-NTs. The Poisson's ratio,  $\nu$ , of PCF-G-NT (6, 0) and (0, 7) are calculated by [23]:

$$\nu = -\frac{\varepsilon_R}{\varepsilon_z}, \quad (5)$$

The radial strain ( $\varepsilon_R$ ) and uniaxial strain ( $\varepsilon_z$ ) are defined in terms of strain mechanical load. The uniaxial strain in  $z$ -direction can be measured from the rate of deformation in PCF-G-NTs (6, 0) and (0, 7). The length ( $L$ ) of PCF-G-NTs (6, 0) and (0, 7) is divided into equal-size slabs with thickness ( $\Delta L = \frac{L}{n}$ ). The uniaxial strain load in  $z$ -direction is then calculated by:

$$\varepsilon_R = \frac{R_{\varepsilon_z}^{(average)} - R_0^{(average)}}{R_0^{(average)}}, \quad (6)$$

where,  $R_{\varepsilon_z}^{(average)}$  is the average PCF-G-NTs (6, 0) and (0, 7) radius at the uniaxial strain load  $\varepsilon_z$ . The  $R_0^{(average)}$  is the average of the PCF-G-NTs radius at the equilibrium,  $\varepsilon_z = 0$ , where:

$$R_{\varepsilon_z}^{(average)} = n^{-1} \sum_{i=1}^n R_i^{(slab)}|_{\varepsilon_z}. \quad (7)$$

In Eq. 7,  $R_i^{(slab)}|_{\varepsilon_z}$  is the average radius of the  $i$ -esim circular slab of the PCF-G-NTs (6, 0) and (0, 7) at uniaxial strain  $\varepsilon_z$ .  $R_i^{(slab)}$  is the average of the distance of each slab composed by carbon atoms to its center of mass. Is calculated by:

$$R_i^{(slab)} = M^{-1} \sum_{\alpha=1}^N r_\alpha, \quad (8)$$

where,  $r_\zeta$  is given by the mathematical expression:

$$r_\alpha = \sqrt{(x_\beta - x_{CM})^2 + (y_\beta - y_{CM})^2}. \quad (9)$$

The Eq. 9,  $x_\beta$  and  $y_\beta$  are the planar coordinates of the  $\alpha$ -esim carbon atoms, where  $M$  is defined by carbon atoms per slab. The coordinates  $x_{CM}$  and  $y_{CM}$  are the mass center of each slab of PCF-G-NTs (6, 0) and (0, 7). We consider  $\Delta L = 1.5 \text{ \AA}$ . There is reasonable minimum number of atoms at each slab of the radius of the PCF-G-NTs (6, 0) and (0, 7) [24].

### 3. Generation of PCF-graphene-based nanotubes - PCF-G-NTs

The computational construction of PCF-G-NTs is initially done by defining the chiral vector (see Fig.3):

$$\mathbf{C}_h = n\mathbf{a} + m\mathbf{b}, \quad (10)$$

where  $\mathbf{a} = 4.915 \text{ \AA}$  and  $\mathbf{b} = 5.487 \text{ \AA}$  are the lattice vectors and  $n, m$  are integers that characterize the type of chirality. Through this vector we can obtain the diameter of the nanotube:

$$d_t = \frac{|\mathbf{C}_h|}{\pi}. \quad (11)$$

The translational vector is perpendicular to the chiral vector, given by (see Fig.3):

$$\mathbf{T} = t_1 \mathbf{a} + t_2 \mathbf{b}, \quad (12)$$

where  $t_1, t_2$  are integers that can be obtained using the inner product  $\mathbf{C}_h \cdot \mathbf{T} = 0$ , thus

$$\frac{t_1}{t_2} = -\frac{m}{n}, \quad (13)$$

knowing that  $\mathbf{a} \cdot \mathbf{b} = 0$  for the rectangular lattice. The length of the nanotube is given by  $L = |\mathbf{T}|$ . The  $\mathbf{C}_h$  (see Fig.3) and  $\mathbf{T}$  vectors therefore delimit the PCF-G-NTs unit cell. The PCF-G-NTs rectangular lattice allows the construction of PCF-G-NTs zigzag-like,  $(n, 0)$  or  $(0, n)$  chirality. The structural parameters of PCF-G-NTs studied in this work can be viewed in Table 1.

#### 4. Results and discussions

Here, we represent the results of reactive (ReaxFF) classical molecular dynamics (CMD) simulations of the stretching dynamics of PCF-graphene single-layer and PCF-graphene-based nanotubes (PCF-G-NTs) in order to investigate the elastic properties and fracture pattern of these nanostructures in 1D and 2D morphology dimensions. In Fig. 2, we present the bond length distribution analysis for PCF-graphene nanostructure configurations. Notably, the bond lengths exhibit a distribution spanning the range of  $1.42 - 1.50 \text{ \AA}$ . The angle distribution analysis for PCF-graphene nanostructure exhibit a distribution spanning the range of  $112 - 136$ . The Young's modulus, ultimate tensile strength (UTS) and critical strain values obtained by CMD for PCF-graphene single-layer and PCF-G-NTs studied in the research work are presented in Table 2.

Complete nanostructural failure of PCF-graphene single-layer ( $146.22 \times 163.23 \text{ \AA}^2$  (14400 carbon atoms) ranges from  $11.12 - 14.87\%$  ( $x$ -direction) and  $16.51 - 33.37\%$  ( $y$ -direction) of strain. The PCF-G-NTs  $(n, 0)$  ranges from  $22.22 - 39.27\%$  and  $(0, n)$   $12.23 - 25.87\%$  of strain, respectively. On the other hand, different critical strains were observed when comparing graphene single-layer and conventional CNTs. Where the critical strain of graphene single-layer ( $(90 \times 90) \text{ \AA}^2$  with 3656 carbon atoms) with uniaxial stretching applied in the  $x$  direction is  $10.96\%$  and in the  $y$  direction is  $13.24\%$ . For conventional nanotubes these values change from  $16 - 18\%$ , results obtained with the same computational methodology developed here in this work [25, 26]. We attribute the differences due to the nanostructural morphology between PCF-graphene and graphene single-layer, where the PCF-graphene single-layer presents in its nanostructure all carbon atoms threefold coordinated (see Fig. 1). The graphene single-layer, on the other hand, presents densely packed hexagonal carbon atoms in its nanostructural morphology. Thus, like conventional CNTs formed by rolled up a single layer of graphene, also presents a densely packed nanostructural morphology [25, 26]. Therefore, the nanostructural morphology between PCF-graphene and graphene single-layer and nanotubes, present significant differences in their elastic deformation and significantly affect its mechanical properties. The Young's modulus between single-layer

PCF-graphene and nanotubes also show significant differences. The results obtained in our computer simulations show that the Young's Modulus for single-layer PCF-graphene for uniaxial strain in the  $x$  direction ranges from 5651.7 – 4328.6 GPa.Å and in the  $y$  direction 2408.5 – 1934.4 GPa.Å , for temperatures ranges of the 10, 300, 600, 900 and 1200 K. Comparing with the Young's Modulus of graphene single-layer the value is 3350 GPa.Å , considering the thickness of 3.35Å[25]. We can observe that for deformation in the  $x$  direction, the Young's Modulus for the single-layer PCF-Graphene is 40.99% larger than the graphene single-layer. For deformation in the  $y$  direction Young's modulus is 27.78% smaller than the graphene membrane. Our results show that Young's modulus of PCF-graphene single-layer presents changes in its values due to the effects of temperature. In the  $X$  direction the values decrease in 23.41% while in the  $Y$  direction the values decrease in 19.68% . Lu, P. L. (2008), investigated using an empirical force-constant model, the mechanical properties of single wall conventional carbon nanotubes. The results showed that the Young's Modulus CNTs is 970 GPa (or 3249.5 GPa.Å , with thickness of 3.35Å) [27]. Hernandez, E. *et. al* (1998), using a non-orthogonal tight-binding formalism, obtained in research results the Young's Modulus value of CNTs are of the 1080 Gpa (or 3618 Gpa.Å , with thickness of 3.35Å). [28] De Sousa (2021), using the reactive (ReaxFF) classical molecular dynamics method, obtained the Young's Modulus of CNT of the 955 GPa (or 3199.25 Gpa.Å , with thickness of 3.35Å) [26]. Comparing these values, the PCF-G-NTs present a Young's Modulus around 18.63% smaller than the conventional CNTs. The ultimate tensile strength of PCF-graphene single-layer and PCF-GNTs ((0,  $n$ ) and ( $n$ , 0)) are range 1934.4 – 5651.7 GPaÅ , 1850.5 – 2603.3 GPaÅ and, 386.25 – 1280.7 GPaÅ, respectively. All values of the mechanical properties of PCF-graphene-based nanotubes are presented in Table 2.

The mechanical properties PCF-graphene single-layer (uniaxial strain in  $x$ -direction and  $y$ -direction at room temperature) and PCF-GNTs ((0,  $n$ ) and ( $n$ , 0)) at room temperature) are presented follow. The nanostructural failure (fracture pattern) processes can be better understood following the fully atomistic molecular dynamics of the temporal evolution of the von Mises stress distributions from the snapshots of the tensile stretch, see Figs. 5, 8 and 14, respectively. From the results of the computational simulations presented in these figures, it is possible to observe a high stress accumulation (in red color) along the 1D and 2D PCF-graphene nanostructures from applied stress through uniaxial stretching of the computer simulation box. This process computational change the shape of the simulation box during a reactive (ReaxFF) molecular dynamics simulations run by *constant engineering strain rate* (see section 2: *computational methodology*). The chemical bonding of PCF-graphene resembles that in the product of a cycloaddition reaction. The space group of the optimized lattice is  $Cmmm$  (space group number of 65), and the carbon atoms occupy two nonequivalent Wyckoff positions [15].

In Fig.5, we present the result of the computational simulation of PCF-graphene single-layer under uniaxial stretching deformation in the  $x$  direction at room temperature. Thus, snapshots of the computational simulations were generated before and during the stretching until the complete mechanical fracture physically characterized by the division of the PCF-graphene single-layer ( $x$ -direction) into two parts. Analyzing the fracture pattern, we can

observe in the results obtained in the computational simulations that the broken of the chemical bonds  $C - C$  are in the bonds of type  $C_1 - C_2$  and  $C_2 - C_1$  approximately parallel to the direction of the uniaxial deformation of the PCF-graphene single-layer (see Fig.4). In all reactive molecular dynamics simulations results, the break bonds of the  $C_2 - C_2$  and  $C_1 - C_1$  was not identified in computational simulations with strain applied in  $x$  direction. In Fig.7, we can observe the pore evolution of PCF-graphene single-layer under uniaxial strain load applied in  $x$ -direction. We can see that porous large deformations but after nanofracture of membrane ( $3.61\text{\AA}$  up to  $3.90\text{\AA}$ ), return to original nanostructural shape, in approximately  $3.58\text{\AA}$ (see Fig.7). As Fig.8 shows the representative nanostructural fully atomic model of PCF-graphene single-layer snapshots under uniaxial stress load in  $y$ -direction at room temperature. In plots (a) - (c), the stretching process of single-layer PCF-graphene, with initiation of nanofracture at 16.30% of strain and complete nanofracture at 16.55% of strain. The small boxes present us an zoomed view of atomistic configuratuion of van der Wall and dynamic bonds from the beginning of the nanofracture until the complete nanofracture of the single-layer PCF-graphene, (d) and (e) at 16.30% of strain. In this theoretical result obtained by reactive CMD simulations showed the representative nanostructural fully atomic model of PCF-graphene single-layer under uniaxial stress load in  $y$ -direction. Panel (a) in Fig. 8 shows the PCF-graphene single-layer at null strain load. In panel (b) initiation of nanofracture with the breaking of some chemical bonds at 16.30% of strain, in (c) the single-layer completely nanofractured at 16.55% of strain, in (d) a zoomed view showed the break of some chemical bonds  $C - C$  and (e) a zoomed view in perspective. In the sidebar, the red color indicates high-stress accumulation, while blue color indicates low-stress accumulation in the PCF-graphene single-layer (see Fig.8). However, to verify the mechanical nanofracture pattern in the PCF-graphene single-layer under uniaxial strain load applied in the  $y$ -direction, we analyzed the stretching evolution of the chemical bonds (see Fig.4). Panels (a)-(d) in Fig. 9 show the beginning of mechanical nanofracture occurs at the bonds  $C_1 - C_2$  and  $C_2 - C_2$  (see Fig.9 (c) and (d)). These bonds are approximately aligned parallel to the direction of uniaxial mechanical stretching in the  $y$ -direction (see Fig.4). In computational reactive CMD, the results showed that the chemical bonds between the canbon atoms  $C_1 - C_1$  and  $C_2 - C_2$ , nanofractures do not influence the mechanical failure in PFC-graphene single-layer, (see Fig.9 (a) and (b)). In Fig.10, we showed the pore evolution of PCF-graphene single-layer under uniaxial strain load applied in  $y$ -direction. We can see that porous large deformations but after nanofracture of membrane ( $3.61\text{\AA}$  up to  $4.16\text{\AA}$ ), return to original nanostructural shape, in approximately  $3.59\text{\AA}$  (see Fig.10). In **supporting information** (attached), we showed the results of snapshots of the stretching process in the  $x$ -direction and  $y$ -direction for temperatures of 10 K, 600 K, 900 K and 1200 K (Figs. **S1**, **S3**, **S5**, **S7**, **S9**, **S11**, **S13** and **S15**). The mechanical failure tear is different for the temperatures presented, compered to that presented for 300 K. In **supplementary movie S1** (em anexo), one may look at the results for streight (in  $x$ -direction and  $y$ -direction) process failure mechanics of PCF-graphene single-layer at temperature 10 K. We also provide in the supplementary material the atomic coordinates for single-layer PCF-graphene and for the PCF-G-NT nanotubes (6, 0) and (0, 7) in the extension  $xyz$  (**see attached supporting information**). The thermodynamic stability of single-layer PCF-graphene and its based nanotubes PCF-G-NT (6, 0) and (0, 7)



is analyzed through the Potential Energy curve ( $Kcal/mol/atom$  vs time (fs)). The stability of the non-equilibrium reactive (ReaxFF) classical molecular dynamics simulations was obtained in the statistical ensemble NVT (*Nose/Hoover thermostat*) during a thermalization time 250000 fs at 300 K (see **supporting information**: Fig.S17, Fig.S18 and Fig.S19 (attached)).

In Fig.11 we present the plots of stress (GPa.Å) versus strain which indicate the response of mechanical load in  $x$ -direction and  $y$ -direction of the PCF-graphene single-layer based on the reactive (ReaxFF) CMD at 10, 300, 600, 900 and 1200 K of temperature. From the graphical representations of panels (a) and (b) in Fig. 10 we can see two regimes, an elastic and a second plastic regime. The elastic regime (linear region in the graphical), the PCF-graphene under load strain is stretched where it does not break chemical bonds. In the plastic region in PCF-graphene single layer we obtained that the totally nanostructural recovery is no longer possible, resulting from permanent deformations. Nevertheless, the response to mechanical load strain shows different results for the  $x$  and  $y$ -directions of strain applied and temperature, as well. For strain applied in the  $x$  direction at 10 K, 300 K and 600 K, the stress-strain curves of PCF-graphene single-layer are similar to brittle materials and/or nanostructures. While for temperatures of 900 K and 1200 K are similar to ductile materials and/or nanostructures. For more information, see the **supporting information** (attached), where we present snapshots related to the stress-strain curve for a better understanding of the mechanical behavior of PCF-graphene single-layer under uniaxial strain load applied in  $x$ -direction (see Figs. **S1** up to **S8**). Panel (b) in Fig.10 shows a graphical representation of the stress-strain curve for PCF-graphene single-layer in the strain applied in the  $y$ -direction. For temperature of 300 K, the results are similar to brittle materials and/or nanostructures, while for 10 K, 600 K, 900 K and 1200 K, the results are similar to ductile materials and/or nanostructures. In **supporting information** (attached), where we present snapshots related to the stress-strain curve for a better understanding of the mechanical behavior of PCF-graphene single-layer under uniaxial strain load applied in  $y$ -direction (see Figs. **S9** up to **S16**).

In Figs.12 and 13, we present the plots of stress (GPa.Å) versus strain which indicate the behavior of the response of uniaxial mechanical load in  $z$ -direction of the PCF-graphene-based nanotubes (PCF-G-NTs)  $(n, 0)$  and  $(0, n)$ , obtained based on the reactive (ReaxFF) CMD at 10, 300, 600, 900 and 1200 K of temperature. As shown, the results are similar to brittle materials and/or nanostructures. Table 1 shows the structural specifications of all PCF-G-NTs  $(0, n)$  and  $(n, 0)$  studied in this work. Fig.14 shows representative snapshots of the nanostructural fully atomic model of PCF-graphene-based nanotubes  $(0, 7)$  and  $(6, 0)$  chirality, respectively, under uniaxial stress load applied in  $z$ -direction. Plots (a)-(c) in Fig.13 show the failure mechanical nanofracture mechanics of PCF-G-NT  $(0, 7)$  where (a), (b) and (c) are at null strain load, fully stressed at 20.27% and completely nanofractured at 20.74% of strain load, respectively. The small boxes (e) and (f) in Fig.13 show the break of some chemical bonds  $C - C$  and PCF-G-NT  $(0, 7)$  completely fractured, respectively. In plots (d) and (g) a perspective view of the PCF-G-NT  $(0, 7)$  presented. In addition, plots (h) - (n) present the failure mechanical nanofracture mechanics of PCF-G-NT  $(6, 0)$  so that (h), (i) and (j) are at null strain load, fully stressed at 34.41% and completely nanofractured

at 20.74% of strain load, respectively. Furthermore, the small boxes (l) and (m) in Fig.13 show the break of some chemical bonds  $C - C$  and PCF-G-NT (0, 7) completely fractured, respectively. Finally, the plots (k) and (n) present a perspective view of the PCF-G-NT (6, 0).

Fig.15, shows the graphical Poisson's coefficients representation of PCF-G-NTs (6, 0) and (0, 7) as a function of the uniaxial strain applied in  $z$ -direction. After subjecting PCF-G-NT (6, 0) to a 14% of load mechanical strain, a noticeable decline in the Poisson's coefficient is observed, eventually reaching a remarkable value of 0.20. Conversely, PCF-G-NT (0, 7) Poisson's coefficient even under the same strain load conditions is 0.48.

Using the Poisson's coefficients, we can obtain an elastic property of the PCF-graphene-based nanotubes which studied in this work. The evaluations were done by transversal deformation of the PCF-G-NTs, with homogeneous and isotropic fully atomistic carbon atoms configurations. The results showed that the values for the Poisson's ratio are different between PCF-G-NT (6, 0) and (0, 7). This finding is consistent with the fact that PCF-G-NT (6, 0) and (0, 7) show different nanostructural morphologies.

## 5. Conclusions and remarks

The present study deals the mechanical properties and nanofracture patterns of PCF-graphene single-layer and PCF-graphene-based nanotubes (PCF-G-NT  $(n, 0)$  and  $(0, n)$ ), performed by reactive (ReaxFF) Classical Molecular Dynamics Simulations method. The stress-strain graphical representation behavior of the PCF-graphene was observed to follow two regimes: *(i)* one exhibiting linear elasticity and *(ii)* a plastic ones (involving carbon atom re-hybridization and bond breaking). The PCF-graphene single-layer for strain applied in the  $x$ -direction at 10 K, 300 K and 600 K, are similar to brittle materials and/or nanostructure and for 900 K and 1200 K are similar to ductile materials and/or nanostructures. The PCF-graphene single-layer with strain applied in the  $y$ -direction at temperature of the 300 K, are similar to brittle materials and/or nanostructures, while for 10 K, 600 K, 900 K and 1200 K, are similar to ductile materials and/or nanostructures. The Young's Modulus for PCF-graphene single-layer for uniaxial strain in the  $x$ -direction ranges from 5651.7 – 4328.6 GPa.Å and in the  $y$ -direction 2408.5 – 1934.4 GPa.Å, considering the thickness of 3.35Å. The Young's Modulus for the PCF-graphene single-layer is 40.99% larger than the graphene single-layer. The Young's modulus of the PCF-G-NTs ( $(0, n)$  and  $(n, 0)$ ) are range 1850.5 – 2603.3 GPa.Å and, 386.25 – 1280.7 GPa.Å, respectively. The Poisson's coefficients value representation of PCF-G-NTs (6, 0) and (0, 7) as a function of the uniaxial strain applied in  $z$ -direction (30% of load mechanical strain) are 0.68 and 0.48, respectively.

## 6. Acknowledgements

This work was supported in part by the Brazilian Agencies CAPES, CNPq, FAPESP and FAPEPI. J.M.S acknowledges CENAPAD-SP (Centro Nacional de Alto Desempenho em São Paulo - Universidade Estadual de Campinas - UNICAMP) provided computational support (proj842). R. Kalami, S.A. Ketabi and J.M. De Sousa would like to thank School of Physics, Damghan University, Condensed Matter Physics department.

## References

- [1] A. Hirsch, The era of carbon allotropes, *Nature materials* 9 (11) (2010) 868–871.
- [2] E. H. Falcao, F. Wudl, Carbon allotropes: beyond graphite and diamond, *Journal of Chemical Technology & Biotechnology: International Research in Process, Environmental & Clean Technology* 82 (6) (2007) 524–531.
- [3] K. S. Novoselov, A. K. Geim, S. V. Morozov, D.-e. Jiang, Y. Zhang, S. V. Dubonos, I. V. Grigorieva, A. A. Firsov, Electric field effect in atomically thin carbon films, *science* 306 (5696) (2004) 666–669.
- [4] F. Withers, M. Dubois, A. K. Savchenko, Electron properties of fluorinated single-layer graphene transistors, *Physical review B* 82 (7) (2010) 073403.
- [5] D. C. Elias, R. R. Nair, T. Mohiuddin, S. Morozov, P. Blake, M. Halsall, A. C. Ferrari, D. Boukhvalov, M. Katsnelson, A. Geim, et al., Control of graphene’s properties by reversible hydrogenation: evidence for graphane, *Science* 323 (5914) (2009) 610–613.
- [6] G. Eda, M. Chhowalla, Chemically derived graphene oxide: towards large-area thin-film electronics and optoelectronics, *Advanced materials* 22 (22) (2010) 2392–2415.
- [7] R. R. Nair, W. Ren, R. Jalil, I. Riaz, V. G. Kravets, L. Britnell, P. Blake, F. Schedin, A. S. Mayorov, S. Yuan, et al., Fluorinated graphene: Fluorographene: A two-dimensional counterpart of teflon (small 24/2010), *Small* 6 (24) (2010) 2773–2773.
- [8] M. Z. Flores, P. A. Autreto, S. B. Legoas, D. S. Galvao, Graphene to graphane: a theoretical study, *Nanotechnology* 20 (46) (2009) 465704.
- [9] R. Baughman, H. Eckhardt, M. Kertesz, Structure-property predictions for new planar forms of carbon: Layered phases containing sp<sup>2</sup> and sp atoms, *The Journal of chemical physics* 87 (11) (1987) 6687–6699.
- [10] V. Coluci, S. Braga, S. Legoas, Ds galvao e rh baughman, *Phys. Rev. B* 68 (2004) 035430.
- [11] A. Ivanovskii, Graphynes and graphdienes, *Progress in Solid State Chemistry* 41 (1-2) (2013) 1–19.
- [12] J. M. De Sousa, A. L. Aguiar, E. Girão, A. F. Fonseca, A. Souza Filho, D. Galvão, Computational study of elastic, structural stability and dynamics properties of penta-graphene membrane, *Chemical Physics* 542 (2021) 111052.
- [13] W. Brandão, A. Aguiar, J. M. De Sousa, Atomistic computational modeling of temperature effects in fracture toughness and degradation of penta-graphene monolayer, *Chemical Physics Letters* 778 (2021) 138793.
- [14] J. M. De Sousa, A. Aguiar, E. Girao, A. F. Fonseca, V. Coluci, D. Galvao, Mechanical properties of single-walled penta-graphene-based nanotubes: a dft and classical molecular dynamics study, *Chemical Physics* 547 (2021) 111187.
- [15] Y. Shen, J. Yu, J. Liu, Y. Guo, Y. Qie, Q. Wang, Pcf-graphene: a 2d sp<sup>2</sup>-hybridized carbon allotrope with a direct band gap, *The Journal of Physical Chemistry C* 123 (7) (2019) 4567–4573.
- [16] S. Plimpton, Fast parallel algorithms for short-range molecular dynamics, *Journal of computational physics* 117 (1) (1995) 1–19.
- [17] J. E. Mueller, A. C. van Duin, W. A. Goddard III, Development and validation of reaxff reactive force field for hydrocarbon chemistry catalyzed by nickel, *The Journal of Physical Chemistry C* 114 (11) (2010) 4939–4949.
- [18] J. M. De Sousa, T. Botari, E. Perim, R. Bizao, D. S. Galvao, Mechanical and structural properties of graphene-like carbon nitride sheets, *RSC advances* 6 (80) (2016) 76915–76921.
- [19] J. M. De Sousa, R. Bizao, V. Sousa Filho, A. Aguiar, V. Coluci, N. Pugno, E. Girao, A. Souza Filho, D. Galvao, Elastic properties of graphyne-based nanotubes, *Computational Materials Science* 170 (2019) 109153.
- [20] J. M. De Sousa, G. Brunetto, V. R. Coluci, D. S. Galvao, Torsional “superplasticity” of graphyne nanotubes, *Carbon* 96 (2016) 14–19.
- [21] D. J. Evans, B. L. Holian, The nose–hoover thermostat, *The Journal of chemical physics* 83 (8) (1985) 4069–4074.
- [22] P. Müller, *Fundamentals of stress and strain at the nanoscale level: towards nanoelasticity* (2011).
- [23] L. Wang, Q. Zheng, J. Z. Liu, Q. Jiang, Size dependence of the thin-shell model for carbon nanotubes, *Physical review letters* 95 (10) (2005) 105501.

- [24] W. Brandão, J. M. De Sousa, A. Aguiar, D. Galvão, L. A. Ribeiro Jr, A. F. Fonseca, First-principles and reactive molecular dynamics study of the elastic properties of pentahexoctite-based nanotubes, *Mechanics of Materials* 183 (2023) 104694.
- [25] C. Lee, X. Wei, J. W. Kysar, J. Hone, Measurement of the elastic properties and intrinsic strength of monolayer graphene, *science* 321 (5887) (2008) 385–388.
- [26] J. M. De Sousa, Nanostructures failures and fully atomistic molecular dynamics simulations, in: *Elasticity of Materials*, IntechOpen, 2021.
- [27] J. P. Lu, Elastic properties of carbon nanotubes and nanoropes, *Physical review letters* 79 (7) (1997) 1297.
- [28] E. Hernandez, C. Goze, P. Bernier, A. Rubio, Elastic properties of c and b x c y n z composite nanotubes, *Physical Review Letters* 80 (20) (1998) 4502.

Table 1: Structural parameters of the nanostructural model of PCF-graphene-based nanotubes (PCF-G-NTs) simulated by the reactive Classical Molecular Dynamics Method. The chirality, number of carbon atoms, diameter ( $\text{\AA}$ ) and length ( $\text{\AA}$ ).

Chirality	$n$	Number of Atoms	Diameter ( $\text{\AA}$ )	Length ( $\text{\AA}$ )
$(n, 0)$	4	384	6.26	32.92
	5	480	7.82	32.92
	6	576	9.39	32.92
	7	672	10.95	32.92
	8	768	12.52	32.92
	9	864	14.08	32.92
	10	960	15.64	32.92
$(0, n)$	4	448	6.99	34.40
	5	560	8.73	34.40
	6	672	10.48	34.40
	7	784	12.23	34.40
	8	896	13.97	34.40
	9	1008	15.72	34.40
	10	1120	17.47	34.40

Table 2: Young's Modulus (GPa.Å), Ultimate Tensile Strength (GPa.Å), critical strain  $\epsilon_C$ (%), for PCF-graphene-based single-layer and nanotubes (PCF-G-NTs)

PCF-graphene single-layer				
strain direction	temperature (K)	$Y_{Mod}$ (GPa.Å)	UTS (GPa.Å)	$\sigma_C$ (%)
$x$	10	$5651.7 \pm 42.51$	917.68	11.12
	300	$4839.7 \pm 34.99$	765.89	10.43
	600	$4570.3 \pm 42.32$	654.76	10.33
	900	$4363.4 \pm 50.10$	526.58	18.71
	1200	$4328.6 \pm 53.76$	448.74	14.87
$y$	10	$2408.5 \pm 8.84$	690.50	25.13
	300	$2231.5 \pm 15.77$	551.41	16.51
	600	$2212.5 \pm 18.30$	489.03	33.37
	900	$2036.4 \pm 17.81$	427.37	29.83
	1200	$1934.4 \pm 18.12$	394.17	28.36
PCF-graphene-based nanotubes (PCF-G-NTs) (300 K)				
chirality	$(n, 0), (0, n)$	$Y_{Mod}$ (GPa.Å)	UTS (GPa.Å)	$\sigma_C$ (%)
$(n, 0)$	(4,0)	$386.25 \pm 17.55$	123.78	22.22
	(5,0)	$485.47 \pm 20.95$	123.98	39.27
	(6,0)	$543.54 \pm 31.64$	223.94	28.10
	(7,0)	$688.34 \pm 11.59$	159.78	25.76
	(8,0)	$1246.7 \pm 22.57$	266.00	21.75
	(9,0)	$1093.1 \pm 11.59$	247.35	28.98
	(10,0)	$1280.7 \pm 10.13$	316.83	22.70
$(0, n)$	(0,4)	$1850.5 \pm 58.14$	382.27	12.23
	(0,5)	$1982.0 \pm 52.77$	451.72	25.87
	(0,6)	$1995.4 \pm 26.41$	379.48	18.12
	(0,7)	$2575.3 \pm 27.95$	543.54	20.34
	(0,8)	$2514.4 \pm 37.82$	593.18	21.13
	(0,9)	$2731.6 \pm 32.31$	592.10	21.16
	(0,10)	$2603.3 \pm 33.65$	588.15	24.07

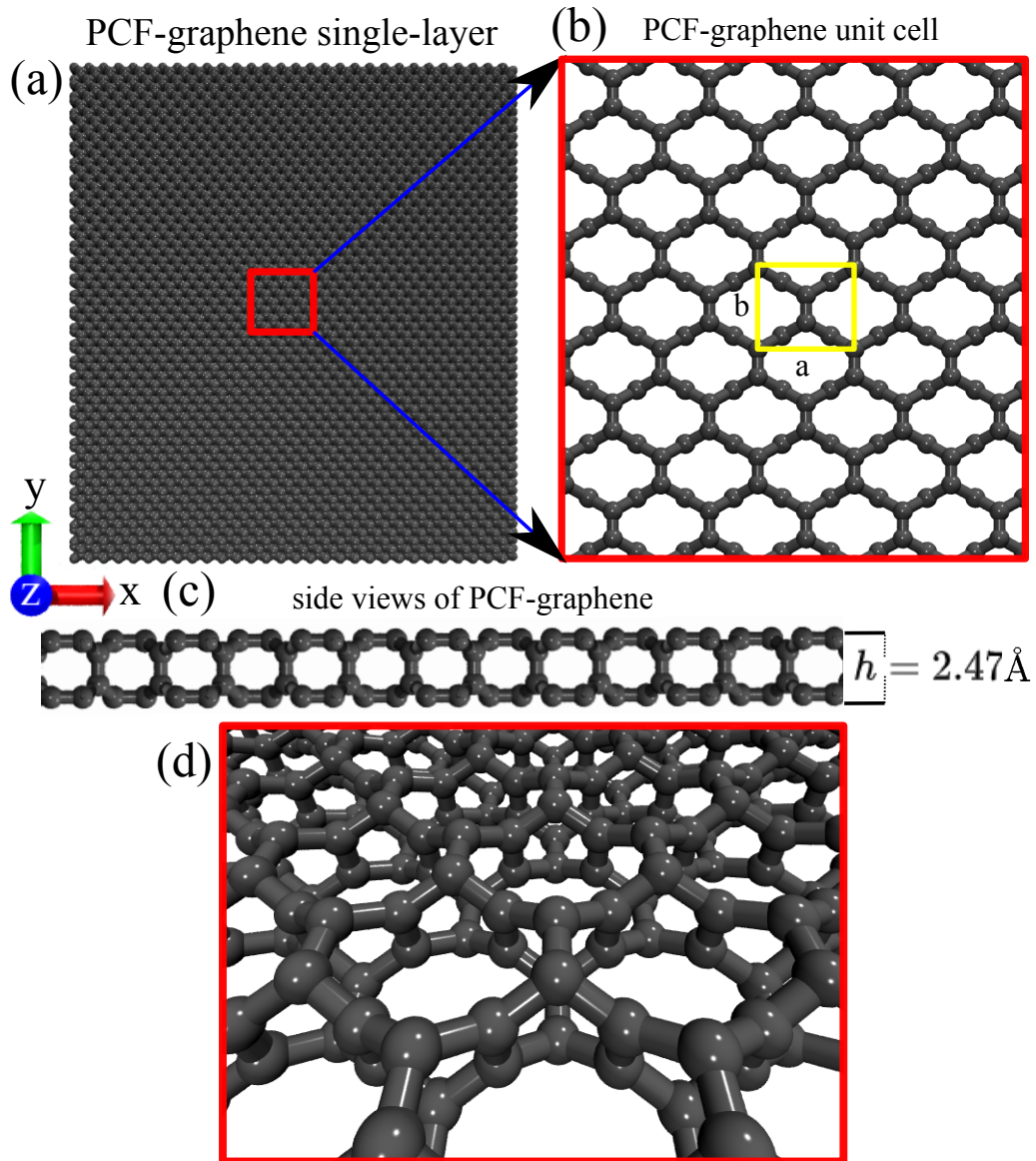


Figure 1: Representative nanostructural fully atomic model of PCF-graphene single-layer (a) Frontal view in the van der Waals representation. In (b), a zoomed of PCF-graphene single-layer show the carbon atoms and dynamics bonds viewer. The yellow rectangle represents the unit cell, where  $a = 4.915 \text{ \AA}$  and  $b = 5.487 \text{ \AA}$ . (c) Side view of PCF-graphene single-layer and, (d) a perspective view of PCF-graphene single-layer.

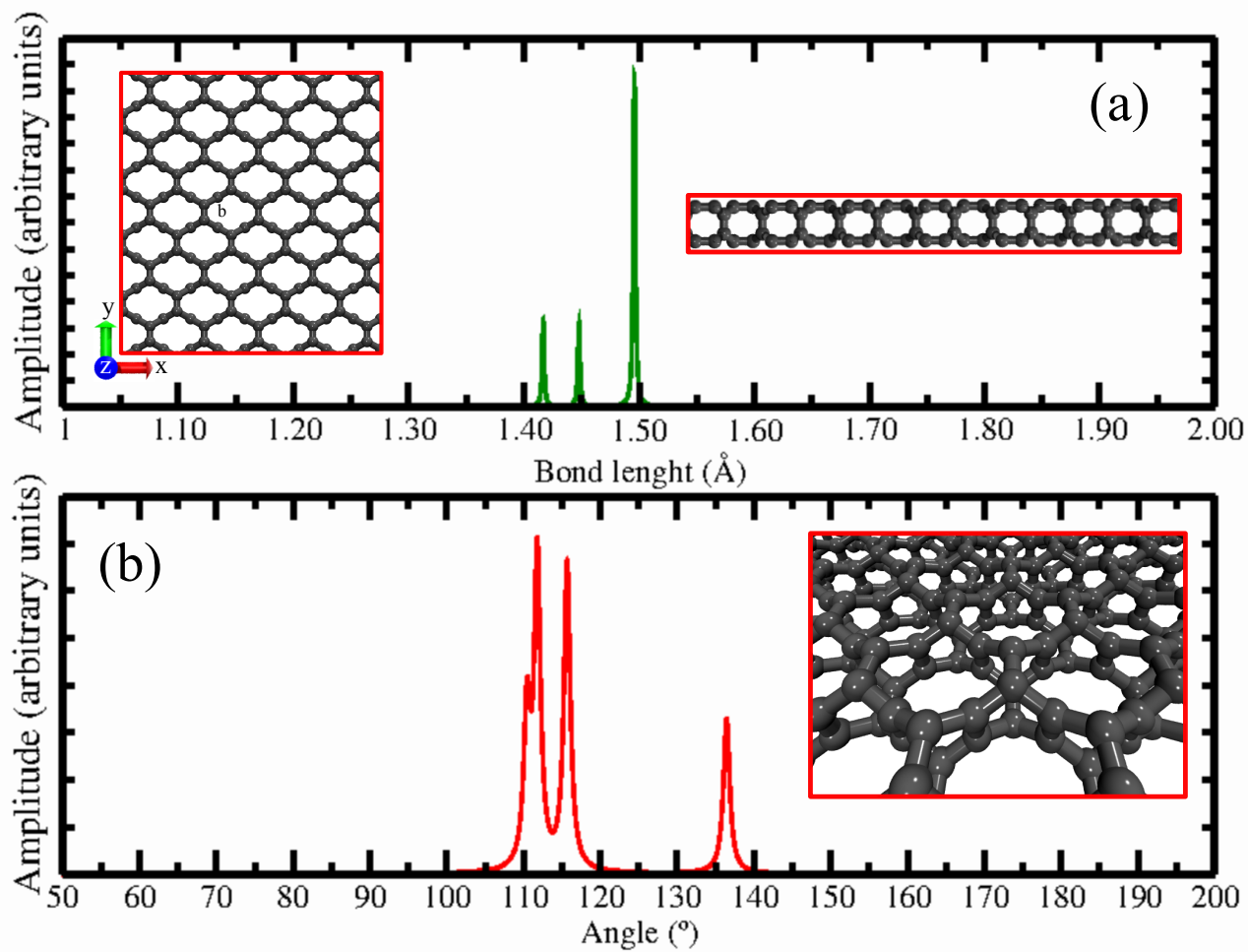


Figure 2: Graphical representation of the evolution of bond length (a) and bond angle (b) of the nanostructural PCF-graphene minimized by ReaxFF set parameter [17].



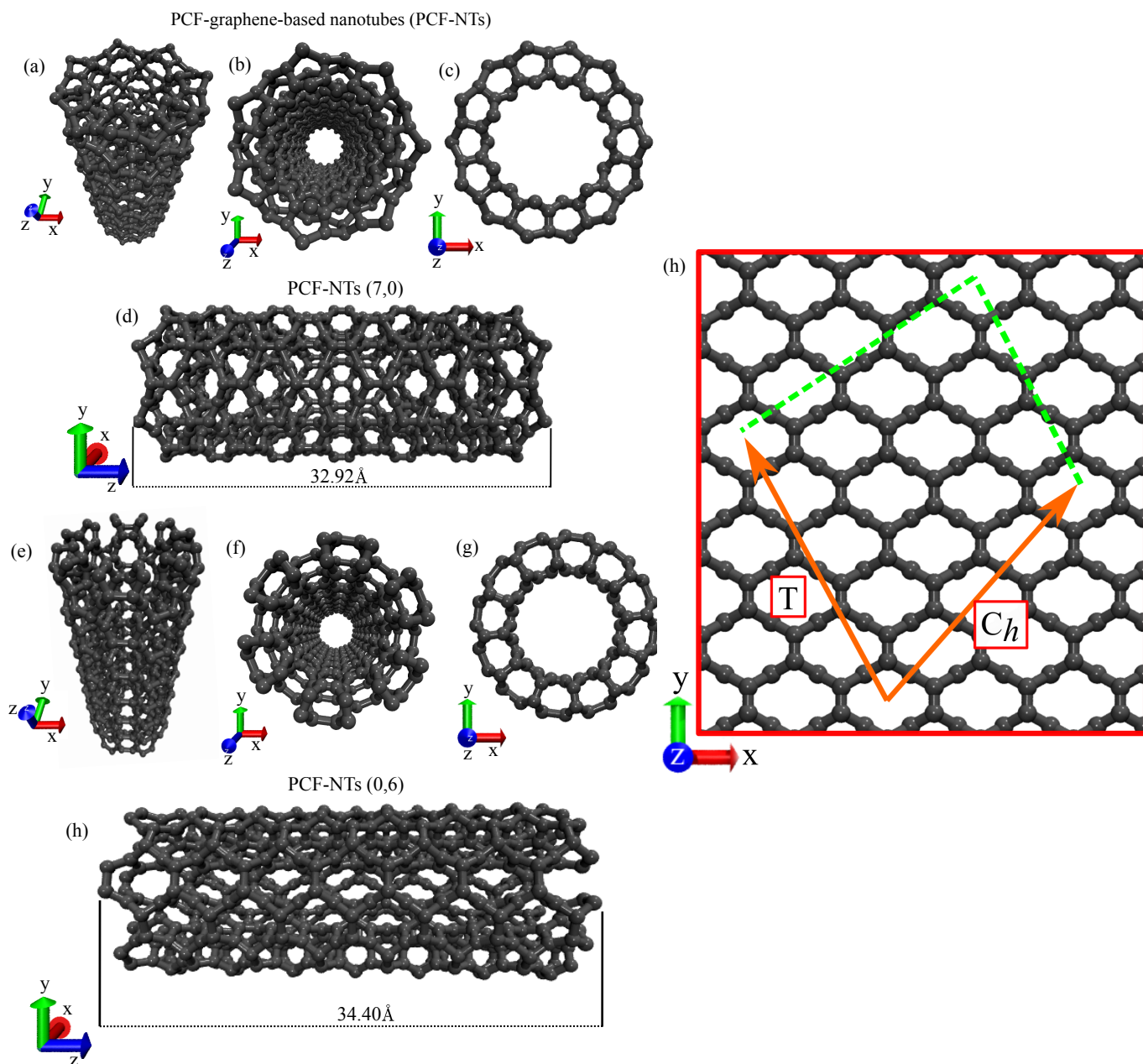


Figure 3: Fully atomistic model illustration of the PCF-graphene nanostructure based nanotubes PCF-G-NT. In viewer module rendered by VMD of the PCF-G-NT (0,7) in (a) longitudinal, (b) perspective, (c) orthographic and (d) length, respectively. In viewer module rendered by VMD of the PCF-G-NT (6,0) in (e) longitudinal, (f) perspective, (g) orthographic and (h) length, respectively. In (i) representation of the chiral ( $\mathbf{C}_h$ ) and translational ( $\mathbf{T}$ ) vectors for a PCF-G-NTs.

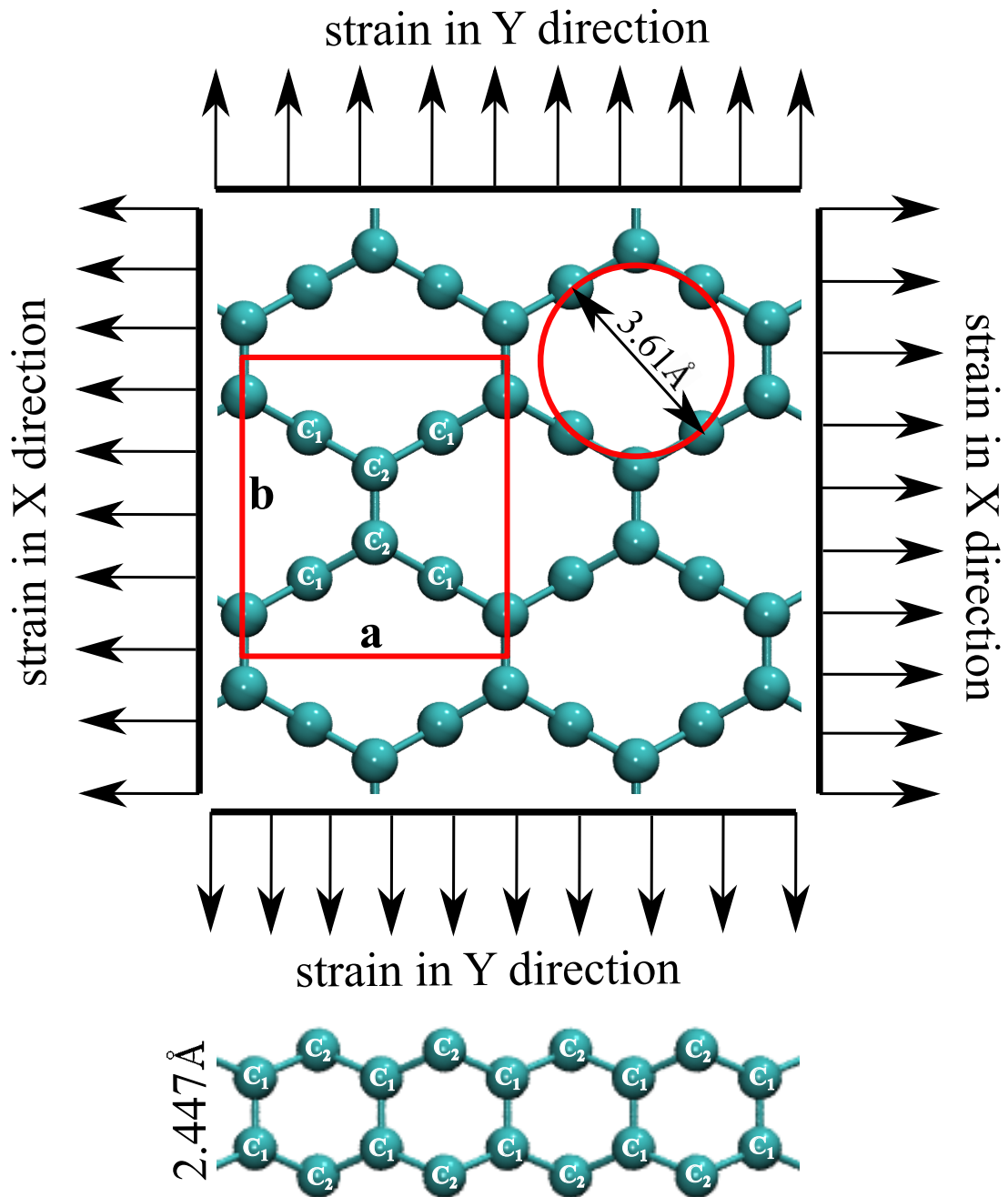


Figure 4: Schematic representation of strain applied directions  $X$  and  $Y$  of the PCF-graphene single-layer. A top and side views of the atomic configuration of PCF-graphene single-layer. The full line rectangle in red color represents the unit cell ( $a=4.915\text{\AA}$  and  $b= 5.487\text{\AA}$ ). The length bonds  $C_1 - C_1$  is  $1.42\text{\AA}$  ,  $C_2 - C_2$  is  $1.45\text{\AA}$  ,  $C_2 - C_1$  is  $1.50\text{\AA}$  and  $C_1 - C_2$  is  $1.50\text{\AA}$  .

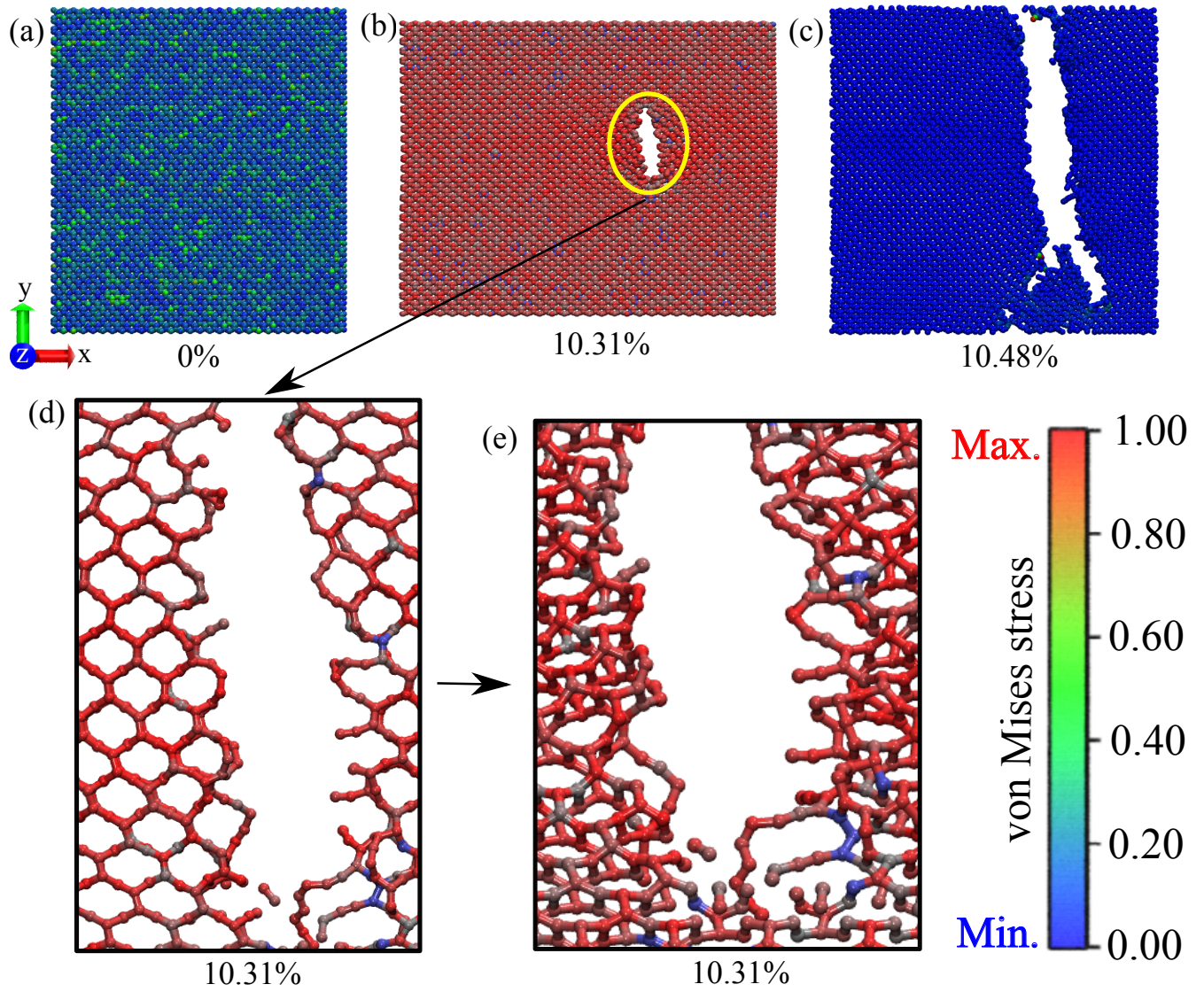


Figure 5: Representative nanostructural fully atomic model of PCF-graphene single-layer under uniaxial stress load in  $X$  direction at room temperature. In (a) at 0% of strain, in (b) initiation of nanofracture with the breaking of some chemical bonds at 10.31% of strain, in (c) the single-layer completely nanofractured in the morphological configuration divided into two parts at 10.48% of strain, in (d) a zoomed view showed the break of some chemical bonds  $C - C$  at 10.31% of strain and (e) a zoomed view in perspective. In the sidebar located on the right side, the red color indicates high-stress accumulation, while blue color indicates low-stress accumulation in the PCF-graphene single-layer.

## Uniaxial strain applied in X direction

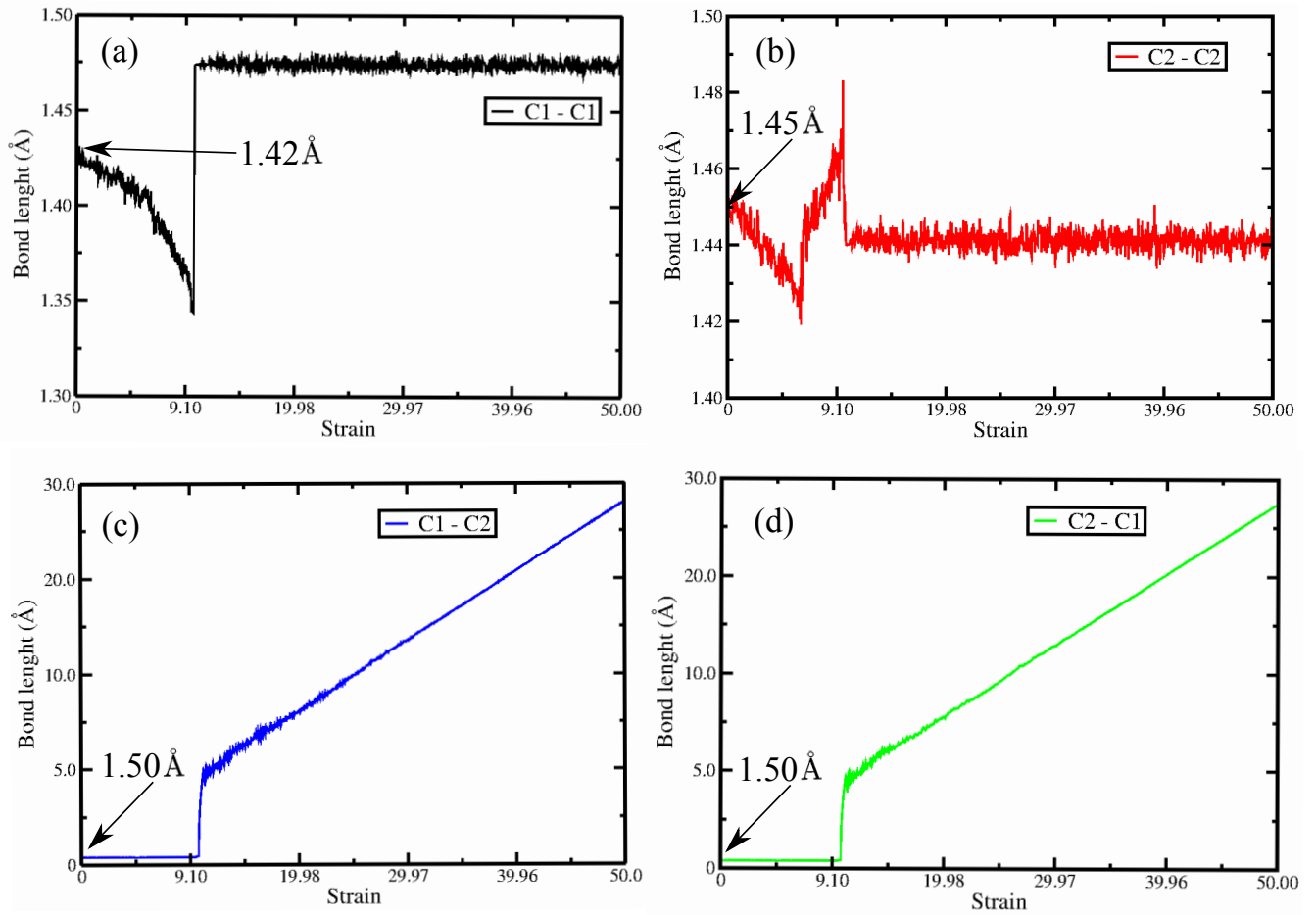


Figure 6: Bond length evolution with strain for PCF-graphene single-layer with uniaxial strain applied in  $X$  direction at temperature 10 K. In (a) chemical bond strain evolution for  $C_1 - C_1$ , in (b) for  $C_2 - C_2$ , (c)  $C_1 - C_2$  and (d)  $C_2 - C_1$ . In Figure 4 is indicated the labeling of each  $C_i$  carbon atom.

### Uniaxial strain applied in X direction

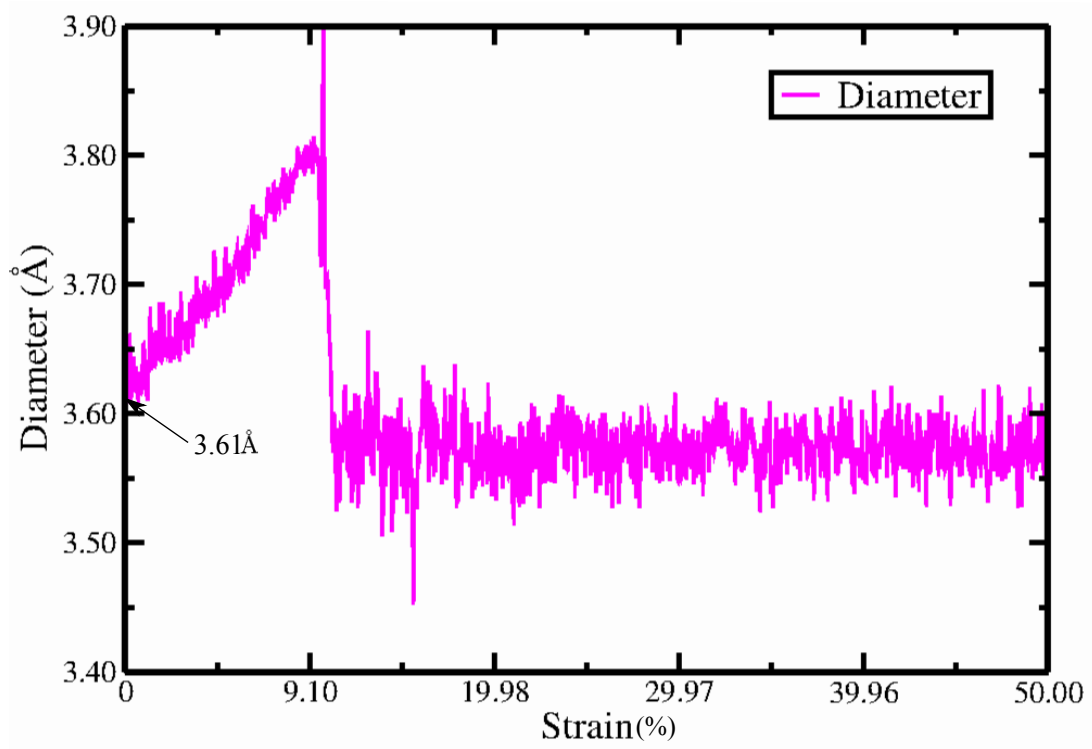


Figure 7: Diameter length evolution with strain for PCF-graphene single-layer with uniaxial strain applied in  $X$  direction at  $10K$  temperature. See Figure 4 is indicated the diameter represented by the circle in red color.

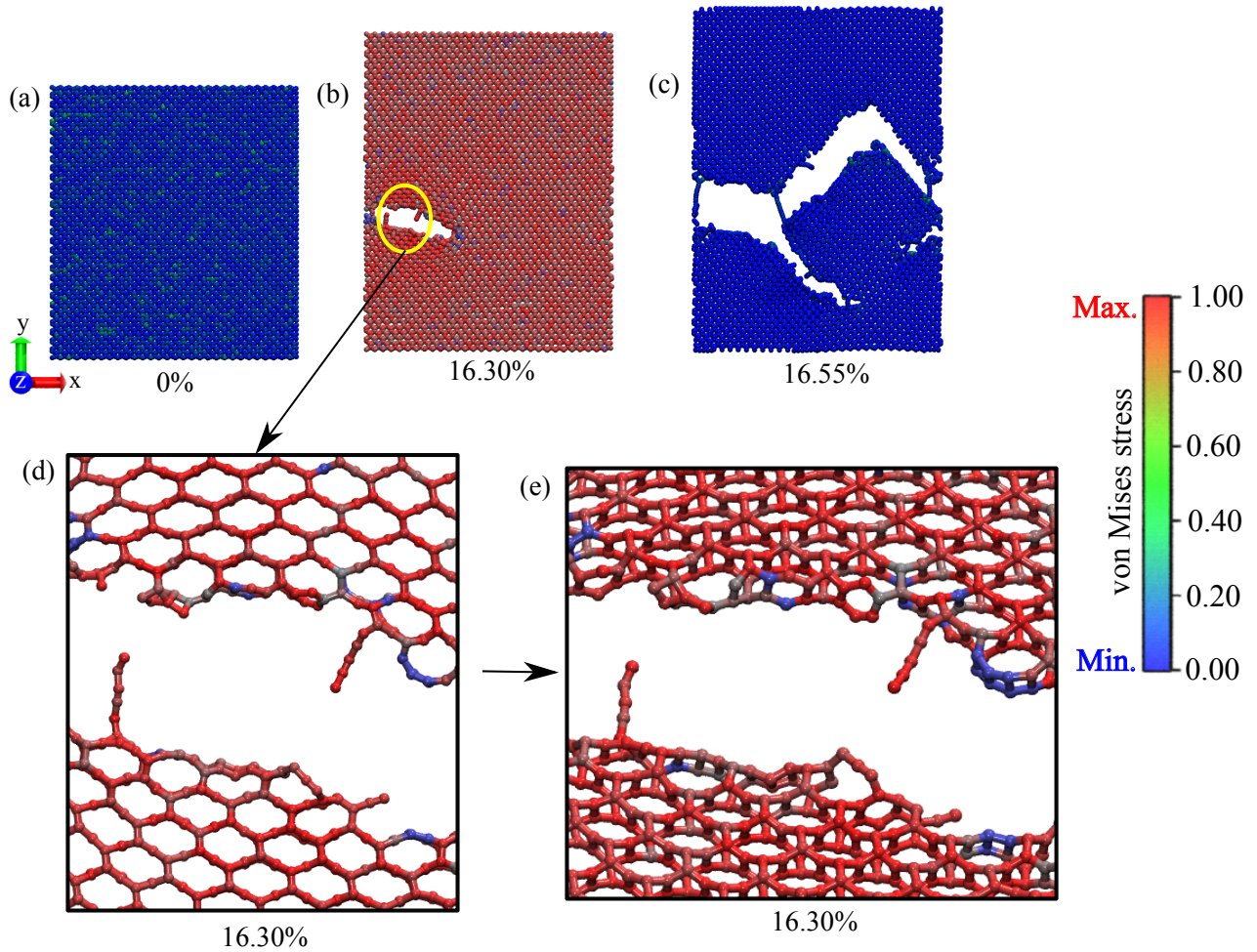


Figure 8: Representative nanostructural fully atomic model of PCF-graphene single-layer under uniaxial stress load in  $Y$  direction. In (a) at 0% of strain, in (b) initiation of nanofracture with the breaking of some chemical bonds at 16.30% of strain, in (c) the single-layer completely nanofractured at 16.55% of strain, in (d) a zoomed view showed the break of some chemical bonds  $C - C$  and (e) a zoomed view in perspective. In the sidebar located on the right side, the red color indicates high-stress accumulation, while blue color indicates low-stress accumulation in the PCF-graphene single-layer.

## Uniaxial strain applied in Y direction

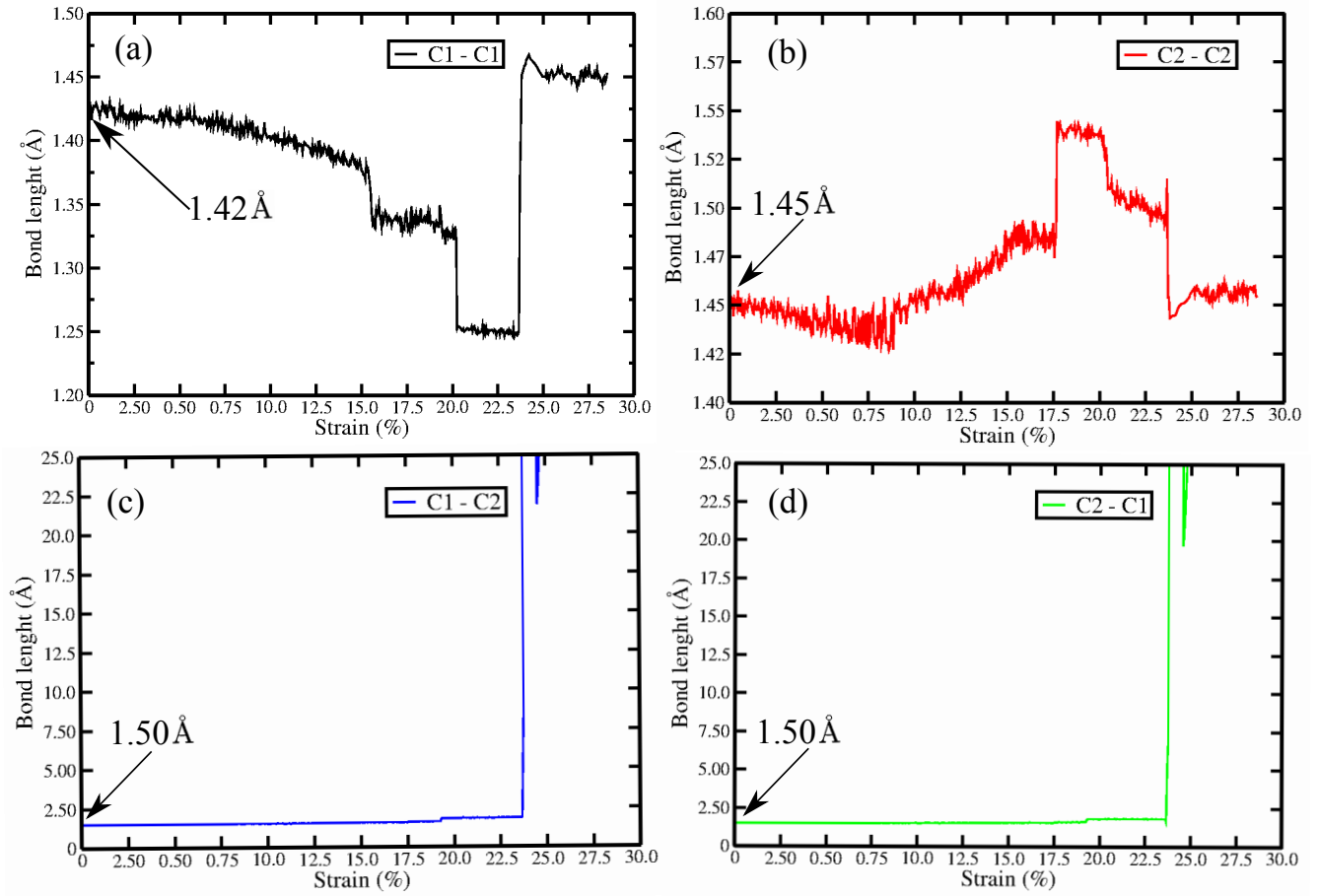


Figure 9: Bond length evolution with strain for PCF-graphene single-layer with uniaxial strain applied in Y direction at temperature 10 K. In (a) chemical bond strain evolution for  $C_1 - C_1$ , in (b) for  $C_2 - C_2$ , (c)  $C_1 - C_2$  and (d)  $C_2 - C_1$ . In Figure 4 is indicated the labeling of each  $C_i$  carbon atom.

### Uniaxial strain applied in Y direction

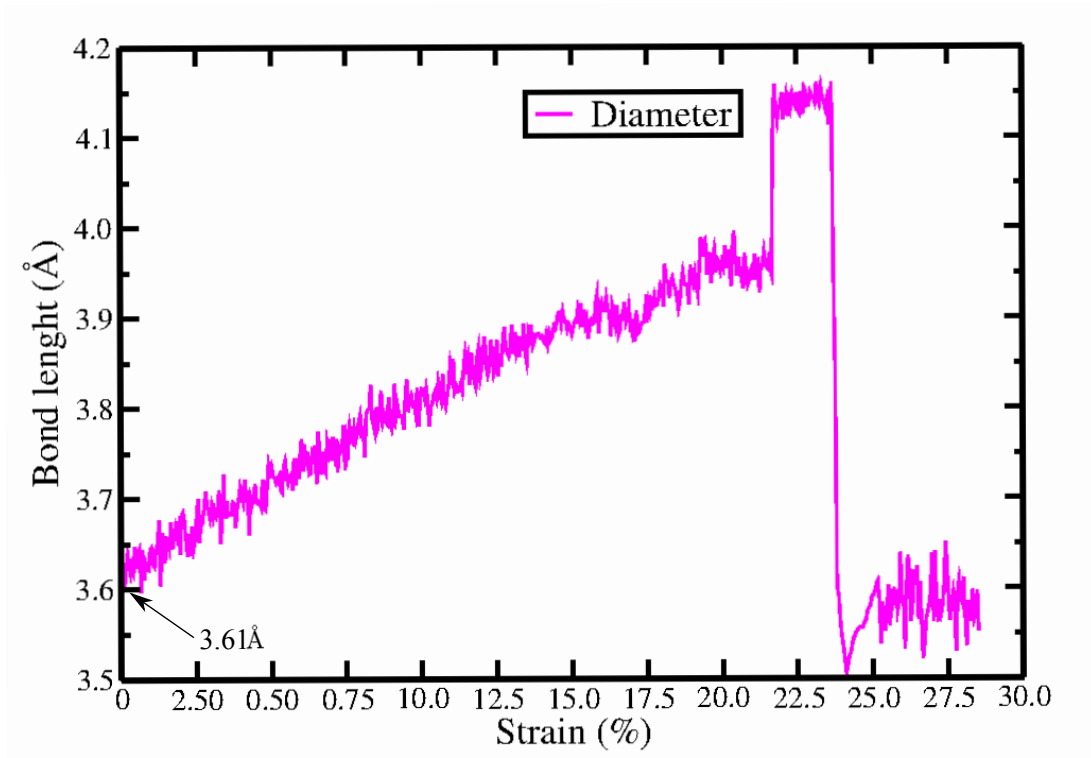


Figure 10: Diameter length evolution with strain for PCF-graphene single-layer with uniaxial strain applied in Y direction at 10K temperature. See Figure 4 is indicated the diameter represented by the circle in red color.



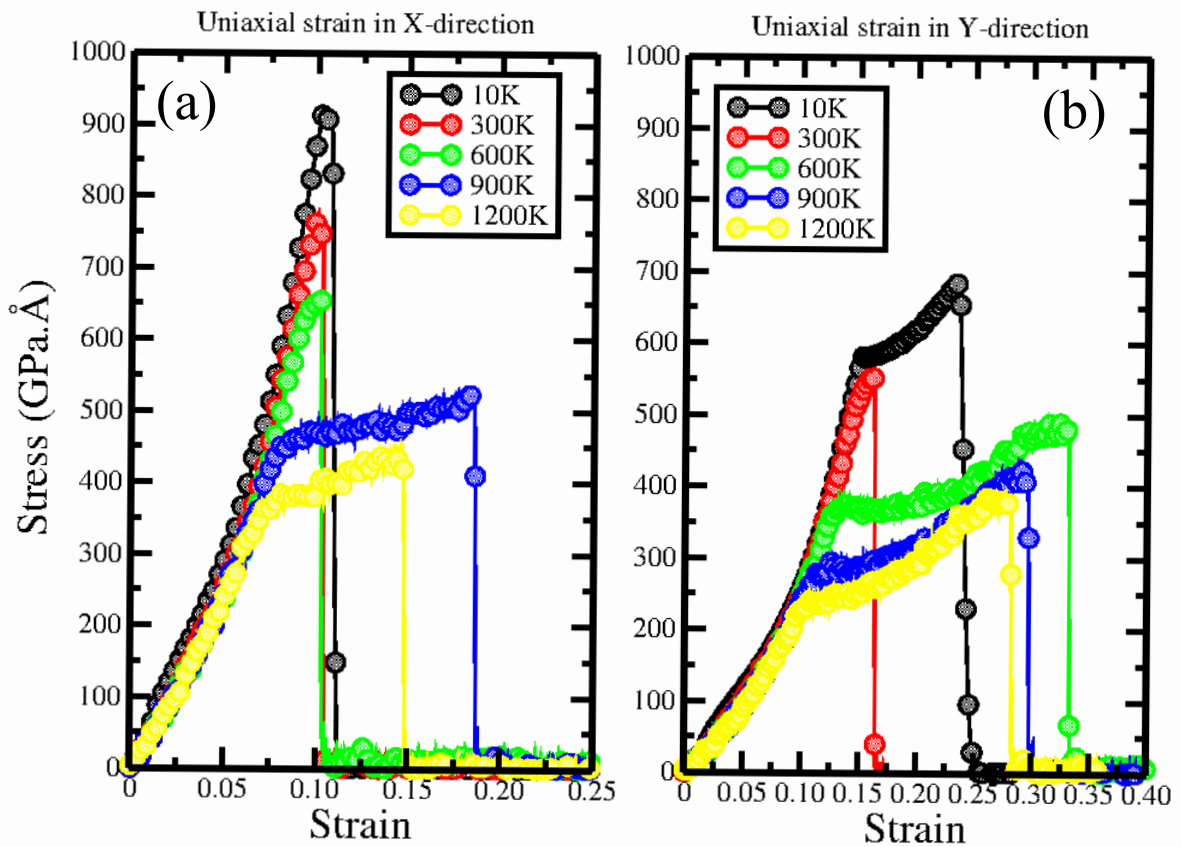


Figure 11: PCF-graphene single-layer stress-strain curve predicted by Classical Molecular Dynamics Simulations Method calculations. In (a) we have the results of the stress-strain curves for uniaxial stress applied in the  $X$  direction for temperatures of 10K, 300K, 600K, 900K and 1200K. In (b) we have the results of the stress-strain curves for uniaxial stress applied in the  $Y$  direction for the same temperatures.

## PCF-graphene-based nanotubes (PCF-G-NTs) - (0,n)

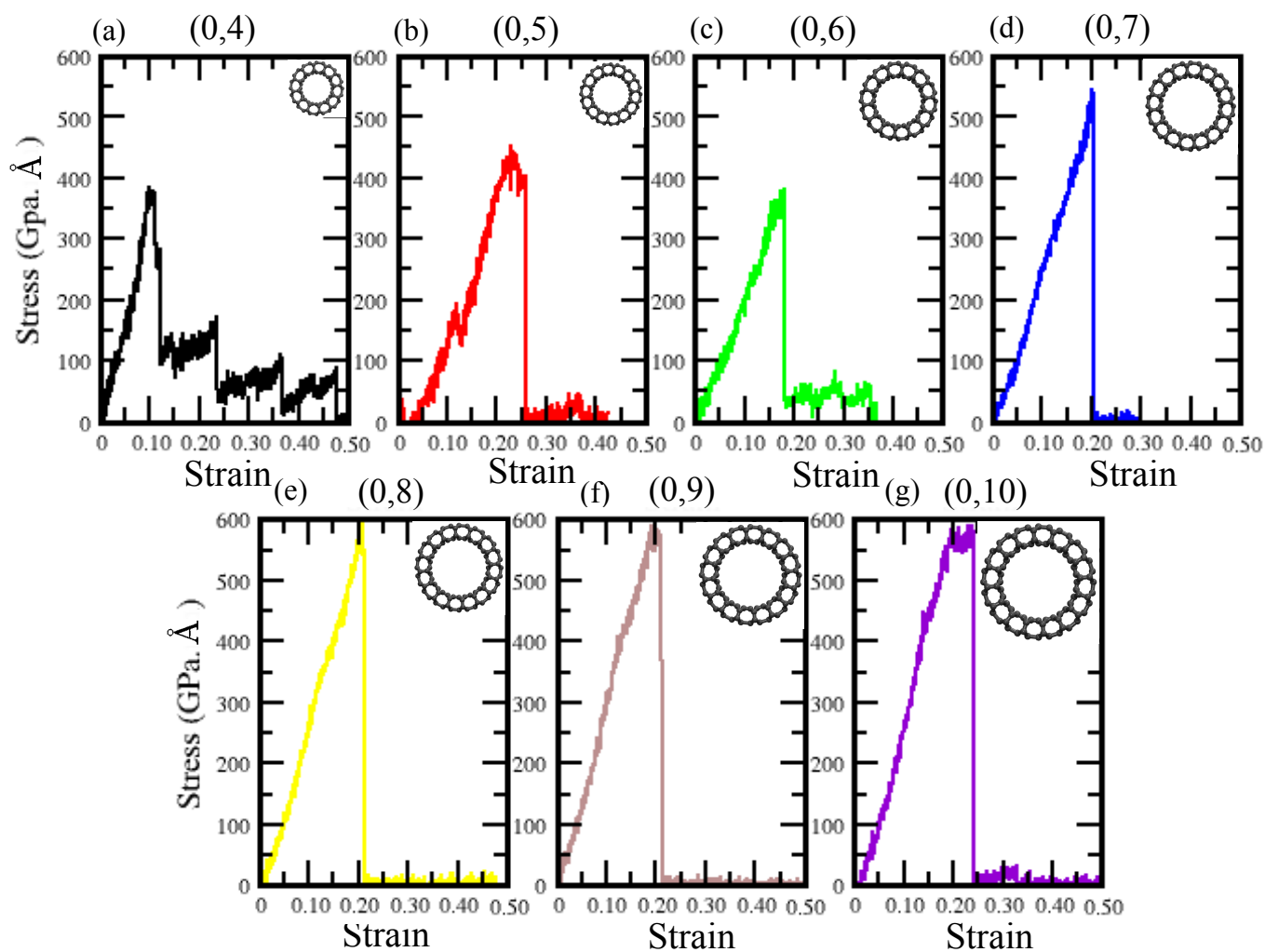


Figure 12: PCF-graphene-based nanotubes (PCF-G-NTs) stress-strain curve predicted by Classical Molecular Dynamics Simulations Method calculations. We have the results of the stress-strain curves for uniaxial stress applied in the  $Z$  direction at room temperature. (a) up to (g) PCF-G-NTs (0,4) up to (0,10) chirality, respectively.

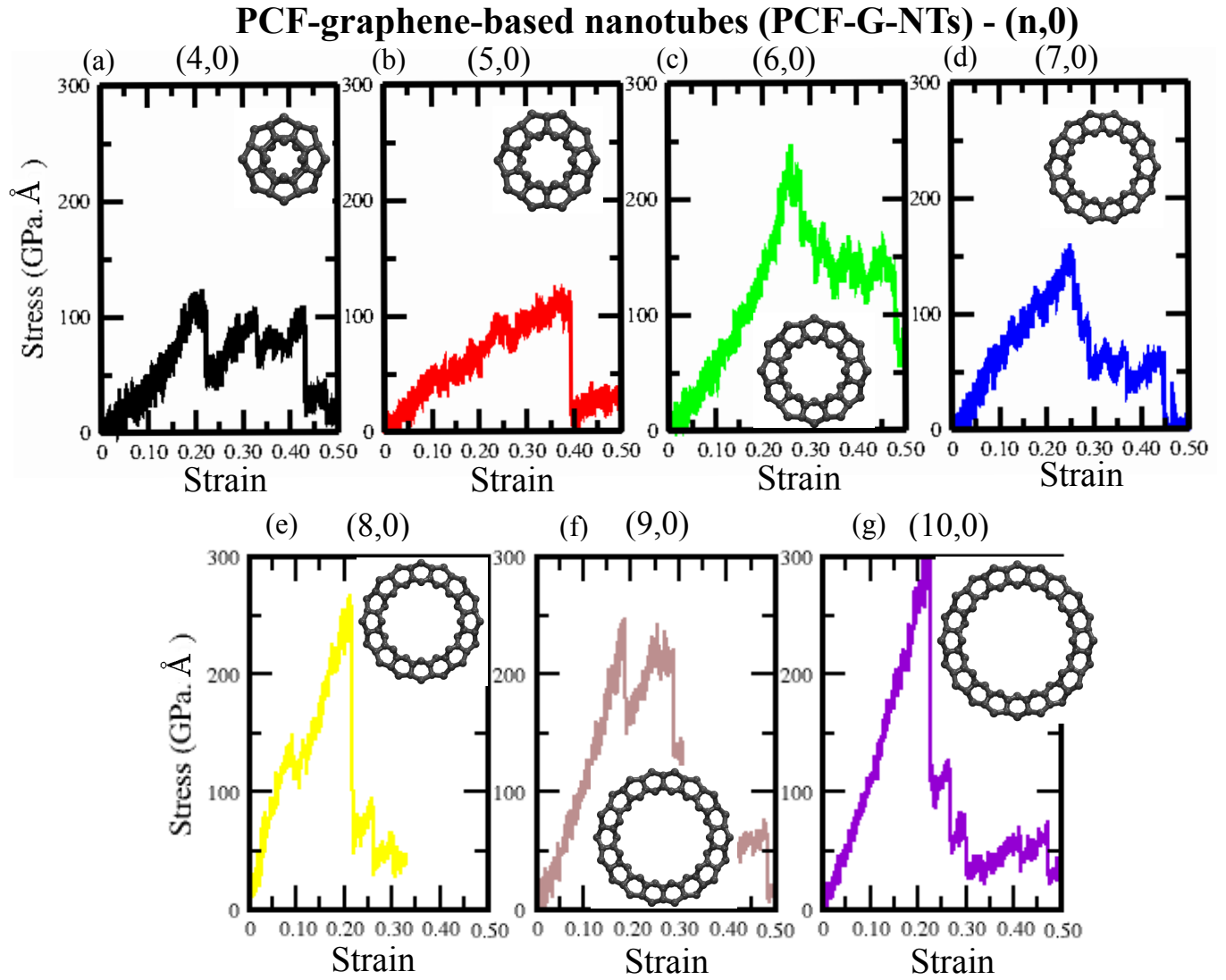


Figure 13: PCF-graphene-based nanotubes (PCF-G-NTs) stress-strain curve predicted by Classical Molecular Dynamics Simulations Method calculations. We have the results of the stress-strain curves for uniaxial stress applied in the Z direction at room temperature. (a) up to (g) PCF-G-NTs (4,0) up to (10,0) chirality, respectively.

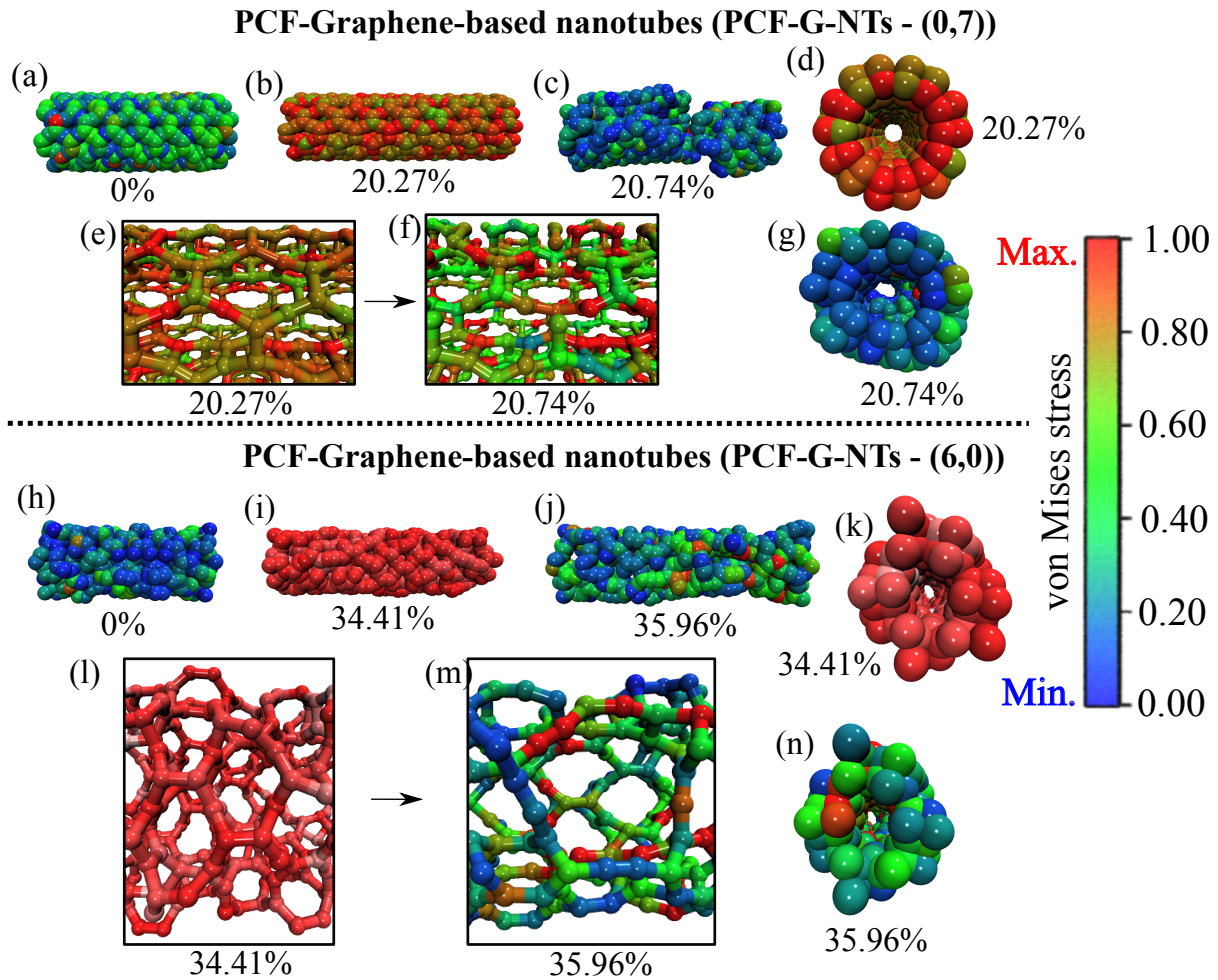


Figure 14: Representative nanostructural fully atomic model of PCF-graphene-based nanotubes (0,7) and (6,0) chirality, respectively, under uniaxial stress load applied in  $Z$  direction. In (a) PCF-G-NTs (0,7) at 0% of strain, in (b) highly tensioned at 20.27% of strain, in (c) the PCF-G-NTs (0,7) completely nanofractured at 20.74% of strain, in (d) and (g) a perspective view of PCF-G-NTs (0,7) at 20.75% and 20.74% of strain, respectively. In (e) the PCF-G-NTs (0,7) with high tensile load showing chemical bonds before mechanical nanofracture, in (f) showed the nanofracture pattern of PCF-G-NTs (0,7). In (h) PCF-G-NTs (6,0) at 0% of strain, (i) highly tensioned at 34.41% of strain, in (j) the PCF-G-NTs (6,0) completely nanofractured at 35.96% of strain, in (k) and (n) a perspective view of PCF-G-NTs (6,0) at 34.41% and 35.96% of strain, in (l) the PCF-G-NTs (6,0) with high tensile load showing chemical bonds before mechanical nanofracture at 34.35% of strain and, (m) showed the nanofracture pattern of PCF-G-NTs (6,0).

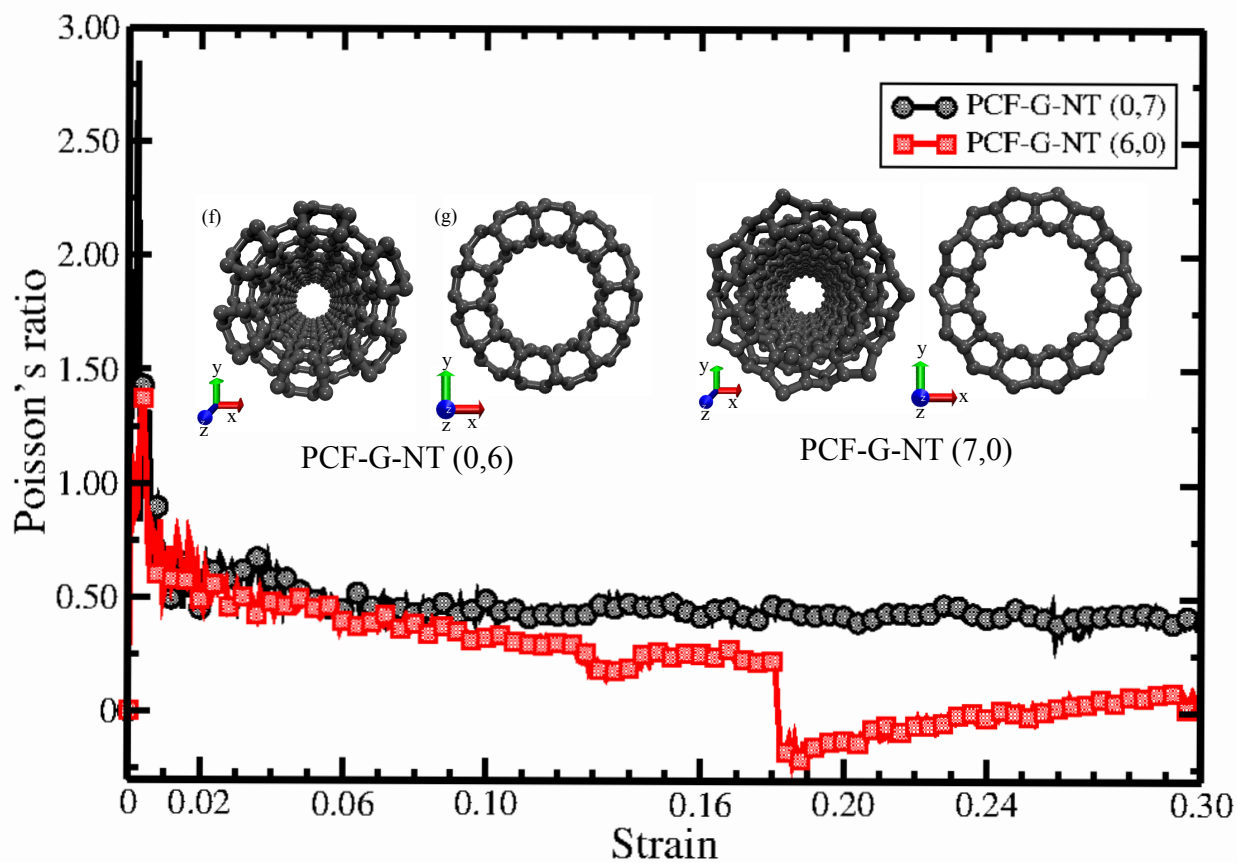


Figure 15: Graphical representation of the Poisson's ratio versus strain obtained by the reactive (ReaxFF) classical molecular dynamics simulations method at room temperature for the PCF-G-NTs (6,0) (red color) and (0,7) (black color).